AIAA JOURNAL
Vol. 47, No. 7, July 2009

Hybrid Continuum/Molecular Simulations of Transient Gas Flows with Rarefaction

Giannandrea Abbate and Chris R. Kleijn*
Delft University of Technology, 2628 BW Delft, The Netherlands
and
Barend J. Thijsse†
Delft University of Technology, 2628 CD Delft, The Netherlands

DOI: 10.2514/1.42111

An adaptively coupled continuum-molecular approach for compressible viscous flows in transient calculations is presented. The continuum domain is described by the unsteady compressible Navier–Stokes equations, and the molecular domain is solved by direct simulation Monte Carlo. A strategy is described to extend the overlapped Schwarz method with Dirichlet–Dirichlet boundary-condition coupling procedure to transient simulations. The method has been successfully validated against full direct simulation Monte Carlo results for transient simulations of a one-dimensional shock tube and a two-dimensional pressure-driven slit flow. A sensitivity analysis showed that the used overlapped Schwarz coupling method with Dirichlet–Dirichlet boundary conditions is only weakly sensitive to various parameters (e.g., the exact position of the continuum/molecular interface, the size of the overlap region, and the scatter in the molecular solution), which is a clear advantage over the more commonly used flux-based coupling technique. Another advantage of the chosen coupling method is that the continuum and molecular time steps can be decoupled and that, in general, a coupling time step can be used that is much larger than the molecular time step. The study performed also highlighted a limit of the method: it was found to be necessary to keep the Courant number (based on the coupling time step, the cell size in the continuum region, and the molecular most-probable velocity) below 1 to avoid instabilities.

Nomenclature

C	=	Courant number
C_r	=	most-probable molecular velocity
E	=	noise
h	=	height
Kn	=	Knudsen number
l	=	length
P	=	pressure
P_{1-2}	=	pressure ratio
Q	=	generic flow property
S	=	surface
T	=	temperature
t	=	time
x, y, z	=	spatial coordinates
Δ	=	discreet value; difference
Δt_c	=	mean collision time
ε	=	prescribed small value
λ	=	mean-free-path length
Ω	=	computational domain

Subscripts

coupling	=	hybrid coupling method
CFD	=	computational fluid dynamics method
DSMC	=	direct simulation Monte Carlo method
f	=	fluxes
max	=	maximum value
ref	=	reference value
split	=	limiting value used to split the continuum from the molecular region
sv	=	state variables
T	=	temperature
V	=	velocity
w	=	wall
x	=	in the x direction
y	=	in the y direction
ρ	=	density

Received 10 November 2008; revision received 2 April 2009; accepted for publication 2 April 2009.

*Department of Multi-Scale Physics, J. M. Burgers Centre for Fluid Mechanics, Prins Bernhardlaan 6; C.R.Kleijn@tudelft.nl.

†Department of Materials Science and Engineering, Mekelweg 2; B.J.Thijsse@tudelft.nl.

I. Introduction

IN MANY practical applications, gas flows undergo spatial and/or temporal transitions from continuum low Knudsen number ($Kn < 0.01$) to rarefied high-Knudsen-number ($Kn > 0.05$) regimes (e.g., due to varying pressure or dimensions). Examples include flow around vehicles at high altitudes (particularly reentry of vehicles in a planetary atmosphere [1]), flow through microfluidic gas devices [2], small cold-gas thruster nozzle and plume flows [3], and low-pressure thin-film deposition processes from expanding plasma or gas jets [4].

Because the Navier–Stokes (N–S) equations are an accurate model of the flow for $Kn \ll 1$ only, Navier–Stokes-based computational fluid dynamics (CFD) models can simulate only gas flows with $Kn < 0.01$ (or with modifications of boundary conditions less than 0.1), whereas gas flows with $Kn > 0.05$ can be simulated using particle-based direct simulation Monte Carlo (DSMC) methods. However, because DSMC computational costs scale with Kn^{-4}, they become prohibitively large when the Knudsen number becomes lower than ≈ 0.05.

Therefore, to accurately and efficiently simulate gas flows with continuum-rarefied transition, it is necessary to construct a model that, on one hand, accounts for the molecular nature of the gas flow when needed and, on the other hand, uses a continuum model when allowed. Such a hybrid model will provide sufficient accuracy at the molecular level while being sufficiently efficient to model large-scale devices.

To compute these kinds of flows, different hybrid models have been proposed to couple different kinds of continuum and atomistic

approaches: for instance, molecular dynamics (MD) and N–S equations [5], Boltzmann and Euler equations [6], Boltzmann and N–S equations [7,8], DSMC and Stokes equations [2], DSMC and incompressible N–S equations [9], DSMC and Euler equations [9–12], and DSMC and N–S equations [13–22].

In the current work, we have decided to couple a compressible Navier–Stokes CFD solver in the continuum region (because of its very wide range of applicability compared with, for example, Euler and incompressible N–S equations) to a DSMC algorithm in the rarefied region, because it is the only practical engineering method that can be used in the rarefied regime.

Note that the vast majority of the cited hybrid models can be applied only to steady-state gas flows [2,5–8,14–20], whereas there are only few hybrid models that are suitable to simulate transient gas flows [9–13]. The most common coupling technique for unsteady gas flows [9–13] is a flux-based coupling method with no overlapping between the continuum and the DSMC regions. This approach suffers from three mean disadvantages that reduce its efficiency.

The first disadvantage is that using a flux-based coupling approach, it is not possible to decouple the global (CFD) and molecular (DSMC) time scales [9]. Because the fluxes at the interface between the two approaches must be exchanged every time step, both CFD and DSMC must be run using the same time step, the size of which is to be chosen as the smallest of the two allowed by the CFD solver and the DSMC solver. Because, in general, $\Delta t_{\mathrm{DSMC}} \ll \Delta t_{\mathrm{CFD}}$, this implies the necessity to also run the CFD solver with the same molecular time step, thus reducing the efficiency of the method [9,16,17].

The absence of an overlapping region is a second disadvantage in most of the flux-based methods. Because the exchange of information between the continuum and molecular approaches takes place at the position of their interface, its exact location is important [9,17]. Thus, in a flux-based coupling method, simulation results strongly depend on the interface location.

The third disadvantage is connected with the DSMC statistical scatter involved in determining fluxes, which is much higher than that associated with the macroscopic state variables. As a result, it has been demonstrated that flux-based coupling methods require a high number of samples to reduce the DSMC statistical noise [9].

In the current work, we propose a strategy to efficiently and accurately couple a compressible N–S solver to a DSMC solver for unsteady flows using Dirichlet–Dirichlet boundary-condition coupling with an overlapped Schwarz method [9,15]. In Sec. IV.A.1, we will show that this method overcomes most of the problems described previously. Thus, given the disadvantages of flux-based coupling methods without overlap [9–13], our work is a clear step forward in the evolution of hybrid continuum-molecular approaches.

II. Breakdown Parameter

The first issue in developing a coupled N–S/DSMC method is how to determine the appropriate computational domains for the DSMC and N–S solvers and the proper interface boundary between these two domains. As a criterion for discriminating the continuum from the rarefied regime and for consequently selecting the proper solver, the continuum breakdown parameter $Kn_{\max}$ [23] is employed:

$$Kn_{\max} = \max[Kn_{\rho}, Kn_{V}, Kn_{T}] \tag{1}$$

where Kn_{ρ}, Kn_{V}, and Kn_{T} are evaluated according to

$$Kn_{Q} = \frac{\lambda}{Q_{\mathrm{ref}}} |\nabla Q| \tag{2}$$

where Q is a flow property (density, velocity, or temperature), and its reference value Q_{ref} can either be its local value (for temperature or pressure) or a typical value (for the velocity). In the region in which the continuum breakdown parameter $Kn_{\max}$ exceeds a limiting value Kn_{split}, the N–S equations cannot be applied to accurately model the flow, and DSMC has to be used. In the following section, the strategy implemented for coupling the Navier–Stokes-based CFD code and the DSMC code will be described.

III. Hybrid Coupling Method

The proposed coupling method extends the Schwarz method described in [12,15,24] to transient flows. An extensive description of the method and its validation against analytical, numerical, and experimental data has already been presented in [24,25].

A. Continuum Algorithm: CFD

The CFD code used for solving the Navier–Stokes equations in the low-Knudsen-number regions is an unsteady solver based on a finite volume formulation in compressible form. It uses an explicit first-order time integration in combination with a second-order, spatially accurate, flux-splitting, MUSCL-scheme Riemann solver for the Navier–Stokes equations [26,27]. An explicit scheme, although computationally more expensive, is used because it is more accurate and because computational expenses of the CFD solver are small compared with those of the DSMC solver.

To match the macroscopic viscosity model to results from the variable hard spheres (VHS) model used in the DSMC approach, as described in the next section, temperature-dependent viscosities and thermal conductivities are computed from kinetic theory [28]. The pressure is computed from the ideal-gas law.

B. Molecular Algorithm: DSMC

Direct simulation Monte Carlo is a well-established algorithm for computing rarefied gas dynamics at the level of the Boltzmann equation; the algorithm is described in more detail in [29]. To accurately model viscous effects, the VHS model is used to calculate particle cross sections. For the implementation of inlet or outlet boundary conditions, a buffer zone or particle reservoir approach is used [18]. A Chapman–Enskog distribution is used to create particles in those reservoirs. The Chapman–Enskog distribution is obtained as an approximate solution of the Boltzmann equation and is expressed as a product of a local Maxwellian and a polynomial function of the thermal velocity components. It has been demonstrated that in a hybrid continuum-DSMC method (a Chapman–Enskog distribution, rather than a simple Maxwellian distribution) is required when the viscous fluxes are taken into account [13,18].

C. Coupling Algorithm: Schwarz Method

The proposed coupling method consists of two stages, as illustrated in Fig. 1.

1) The first stage is a prediction stage, in which (step 1 in Fig. 1) the unsteady N–S equations are integrated in time on the entire domain Ω for a coupling time step $\Delta t_{\mathrm{coupling}} > \Delta t_{\mathrm{CFD}} \gg \Delta t_{\mathrm{DSMC}}$.

2) From this predicted solution (step 2 in Fig. 1), the continuum breakdown parameter $Kn_{\max}$ is computed and its values are used to split Ω in the subdomains Ω_{DSMC} ($Kn_{\max} > Kn_{\mathrm{split}} - \Delta Kn$), where the flowfield will be evaluated using DSMC, and Ω_{CFD} ($Kn_{\max} < Kn_{\mathrm{split}}$), where N–S equation will be solved. For Kn_{split}, a value of 0.05 was used. Between the DSMC and CFD regions, an overlap region ($Kn_{\mathrm{split}} - \Delta Kn < Kn_{\max} < Kn_{\mathrm{split}}$) is considered, where the flow is computed with both the DSMC and the CFD solver (Fig. 2). The value ΔKn was varied to vary the overlapping region size (Sec. IV.A.1).

In the second stage, DSMC and CFD are run in their respective subdomains with their own time steps (Δt_{DSMC} and Δt_{CFD}, respectively) for a coupling time step $\Delta t_{\mathrm{coupling}}$. The grid is automatically refined in the DSMC region to respect the DSMC requirements (Δx, Δy, and $\Delta z < \lambda/3$).

First, DSMC is applied (step 3a in Fig. 1). The predicted DSMC region is compared with that of the previous coupling time step. In the cells that belong to both the previous and the predicted DSMC regions, we consider the same molecules of the previous coupling time step, for which the properties were recorded. In these cells, it is important to consider the same molecules of the previous time step rather than sampling them from continuum variables (temperature,

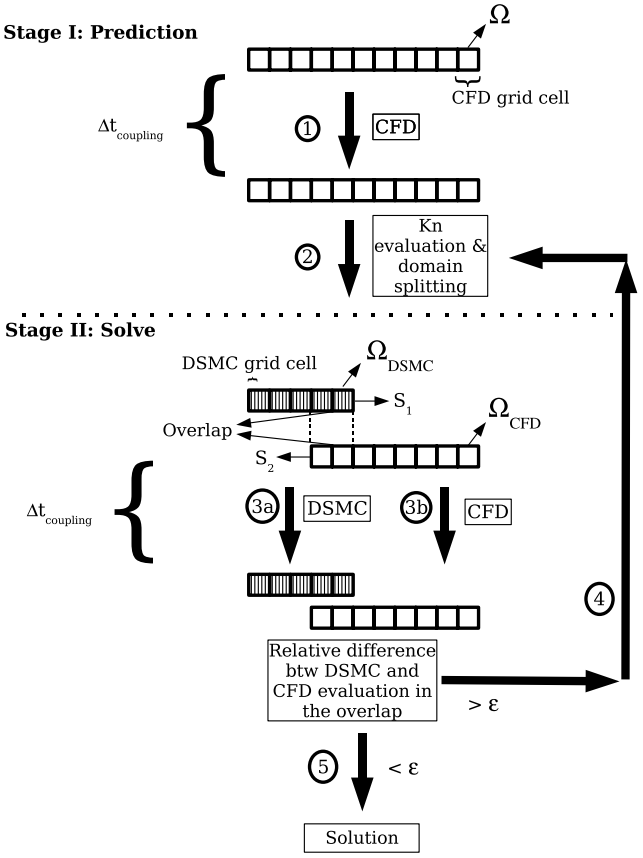

Fig. 1 Scheme of the coupling method.

density, and velocity) with a Maxwellian or a Chapman–Enskog velocity distribution. This is a clear difference with the procedure in [13], in which at every time step, the molecules in the DSMC cells are sampled from continuum variables with a Chapman–Enskog velocity distribution. The use of a Maxwellian or a Chapman–Enskog velocity distribution presumes either equilibrium or near-equilibrium conditions, which is not necessarily true in these cells. Molecules that are in the cells that no longer belong to the DSMC region are deleted, whereas in cells that have changed from being a CFD cell into a DSMC cell, new molecules are created with a Chapman–Enskog velocity distribution, according to the density, velocity, and temperature of the CFD solution at the previous coupling time step. At the CFD/DSMC interface S_1, the boundary conditions to the DSMC region come from the solution in the CFD region. Particle reservoir cells are considered outside the overlap region in which molecules are created according to the density, velocity, temperature, and their gradients in the CFD solution with a Chapman—Enskog velocity distribution.

After running the DSMC (step 3b in Fig. 1), the N–S equations are solved in the CFD region. The boundary conditions to the CFD region at the CFD/DSMC interface S_2 come from the solution in the DSMC region, averaged over the initial CFD grid cells.

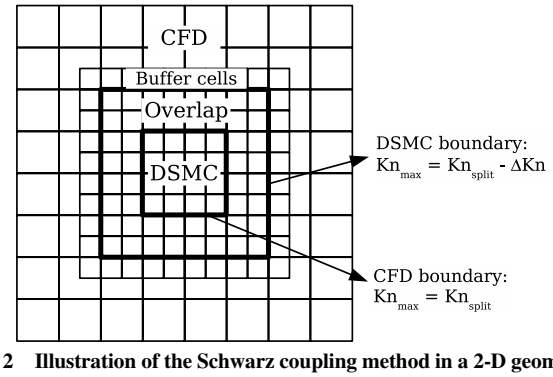

Fig. 2 Illustration of the Schwarz coupling method in a 2-D geometry.

Once both the DSMC and CFD have been run in their respective regions for a time $\Delta t_{\text{coupling}}$, the continuum breakdown parameter $Kn_{\max}$ is reevaluated and a new boundary between the two regions is computed. This second stage (step 4 in Fig. 1) is iterated until (step 5 in Fig. 1) in the overlap region the relative difference between the DSMC and CFD solutions

$$\max_{\text{overlap}}\left|\frac{\Delta Q}{Q_{\text{DSMC}}}\right| = \max_{\text{overlap}}\left|\frac{Q_{\text{CFD}} - Q_{\text{DSMC}}}{Q_{\text{DSMC}}}\right| \tag{3}$$

is less than a prescribed value ε (typically, $\varepsilon \sim 0.001$ [2]). At the end of the described algorithm, the properties of the molecules in the DSMC region are recorded to set the initial conditions in the DSMC region for the next coupling step.

The first clear advantage of using a Schwarz method with Dirichlet–Dirichlet boundary conditions for transient simulations instead of the commonly used flux-based boundary-condition coupling technique [9–13] is the possibility to decouple the global (CFD) and molecular (DSMC) time scales [9]. Because it is possible to couple the continuum and molecular approaches every coupling time step $\Delta t_{\text{coupling}} > \Delta t_{\text{CFD}} \gg \Delta t_{\text{DSMC}}$, in fact, CFD and DSMC can both be run in their respective subdomains with their own time steps (Δt_{DSMC} and Δt_{CFD}, respectively), thus improving the efficiency of the method.

On the contrary, as already highlighted in Sec. I, in the flux-based methods [9–13], the continuum and molecular approaches must be coupled every single time step, the size of which is to be chosen as the smallest one allowed by both the CFD and the DSMC solver. Because the molecular time step is generally much smaller than the continuum time step, then $\Delta t_{\text{coupling}} = \Delta t_{\text{CFD}} = \Delta t_{\text{DSMC}}$.

The second advantage of the Schwarz coupling approach is the use of an overlap region to couple the CFD method to DSMC. Thus, the information exchange between the two methods does not take place at the exact interface position between them, as for the most common flux-based coupling approach [9–13], but through the entire overlap region. For this reason, the simulation results are not strongly influenced by the exact interface location.

The third advantage of using a Schwarz method with Dirichlet–Dirichlet boundary conditions instead of the commonly used flux-based boundary-condition coupling technique [9–13] is that the latter requires a much higher number of samples in the DSMC region than the Schwarz method [9,16,17]. It has been shown [17] that in a DSMC simulation, the relation between the relative noise on fluxes and that on the state variables is

$$E_f \sim \frac{E_{sv}}{Kn} \tag{4}$$

Because at the continuum-molecular interface $Kn \approx 0.01$–0.05, then $E_f \approx 10$–$20E_{sv}$ and 10–20 times more samples are necessary to reduce the DSMC statistical scatter in a flux-based coupling approach than in a Schwarz coupling method with Dirichlet–Dirichlet boundary conditions.

IV. Results and Discussion

In this section, we will apply our hybrid, dynamically coupled, CFD/DSMC solver to one-dimensional and multidimensional transient flows, and we will present a sensitivity analysis of the method to various parameters.

A. Unsteady Shock-Tube Problem

The unsteady coupling method was applied to an unsteady shock-tube test case (Fig. 3). We simulated the flowfield inside a 0.5-m-long tube, connecting two infinitely large tanks filled with argon at different thermodynamic conditions. A membrane at the interface between the first tank and the tube divides the two regions in which the fluid is in different conditions. In the left tank, it is at a pressure $P_1 = 30$ Pa and at a temperature $T_1 = 12,000$ K. In the right tank

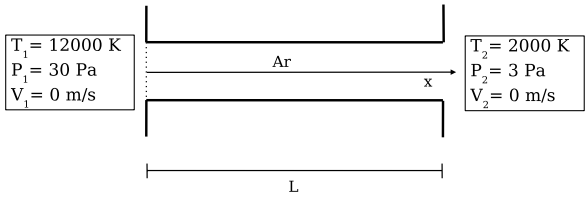

Fig. 3 Shock-tube test case. The dashed line on the left indicates the membrane that is broken at the instant $t = 0$.

and in the tube, it is at a pressure $P_2 = 3$ Pa and at a temperature $T_2 = 2000$ K. These conditions imply that the mean free path (which approximately scales with $T^{1.3}/P$) in the entire domain is $\lambda \approx 0.01$ m.

At the instant $t = 0$, the membrane breaks and the fluid can flow from one region to the other. Two different waves will start traveling in the tube from the left to the right with two different velocities: a shock wave and a contact discontinuity. The shock wave produces a rapid increase of the temperature and pressure of the gas passing through it, whereas through the contact discontinuity, the flow undergoes only a temperature, and not a pressure, variation [30–32].

The thermodynamic conditions inside the infinitely large tanks remain constant. For this reason, the two tanks can be modeled with an inlet and an outlet boundary condition.

Inside the tube, we suppose that the flow is one-dimensional. Upstream (left) from the shock, the gas has a high temperature and relatively high pressure, and gradient length scales are small. Downstream (right) from the shock, both temperature and pressure are much lower, and gradient length scales are large. As a result, the continuum breakdown parameter $Kn_{\max}$ (using local values of Q_{ref}) is high upstream from the shock and low downstream of it. In the hybrid CFD/DSMC approach, DSMC is therefore applied upstream and CFD is applied downstream. For Kn_{split}, a value of 0.05 is used. Rather than setting a value for ΔKn, as discussed in Sec. III, the size of the overlap region is set to 2λ. The initial grid is composed of 100 cells in the x direction and 1 cell in the y direction, whereas the code automatically refines the mesh in the DSMC region to fulfill its requirements.

The coupling time step is chosen as $\Delta t_{\text{coupling}} = 4.0 \times 10^{-6}$ s and ensemble averages of the DSMC solution are made on 30 repeated runs. Note that, due to the time-step decoupling possibility of the Schwarz method, the CFD and DSMC approaches are run with $\Delta t_{\text{CFD}} \approx 2.0 \times 10^{-6}$ s and $\Delta t_{\text{DSMC}} \approx 4.0 \times 10^{-7}$ s, respectively. When time-step decoupling would not have been possible, we should also have run the CFD solver and coupled it to the DSMC solver with a time step of $\mathcal{O}(10^{-7})$ s.

In Figs. 4 and 5, the pressure (Figs. 4a and 5a), temperature (Figs. 4b and 5b), and velocity (Figs. 4c and 5c) inside the tube after 1.5×10^{-5} s and 3.0×10^{-5} s, evaluated with the coupled CFD/DSMC method, are compared with the results of a full DSMC simulation. The latter was feasible because of the 1-D nature of the problem. Results obtained with a full CFD simulation are shown as well. The full DSMC solution is considered to be the most accurate of the three. In Figs. 4d and 5d, the continuum breakdown parameter computed using the coupled method is compared with that same parameter computed with the full CFD simulation.

From the results shown in Figs. 4 and 5, it is clear that the full CFD approach fails due to the high values of the local Knudsen number caused by the presence of the shock. It predicts a shock thickness of $\approx$2 cm, which is approximately 2 times the local mean free path ($\lambda \approx 1$ cm) and therefore unrealistic, because even in continuum conditions, the shock thickness is 1 order of magnitude greater than the mean free path [33]. In the full DSMC approach, therefore, the shock is smeared over almost 10 cm. The results obtained with the hybrid approach are virtually identical to those obtained with the full DSMC solver, but they are obtained in $\sim$25 min on a single processor instead of the $\sim$2.5 h needed for the DSMC simulation. Thus, the hybrid method gives the same accuracy of the DSMC method but in less than one-fifth of the CPU time.

Comparing Figs. 4 and 5, it is also possible to see how the DSMC and CFD regions adapt in time to the flowfield evolution.

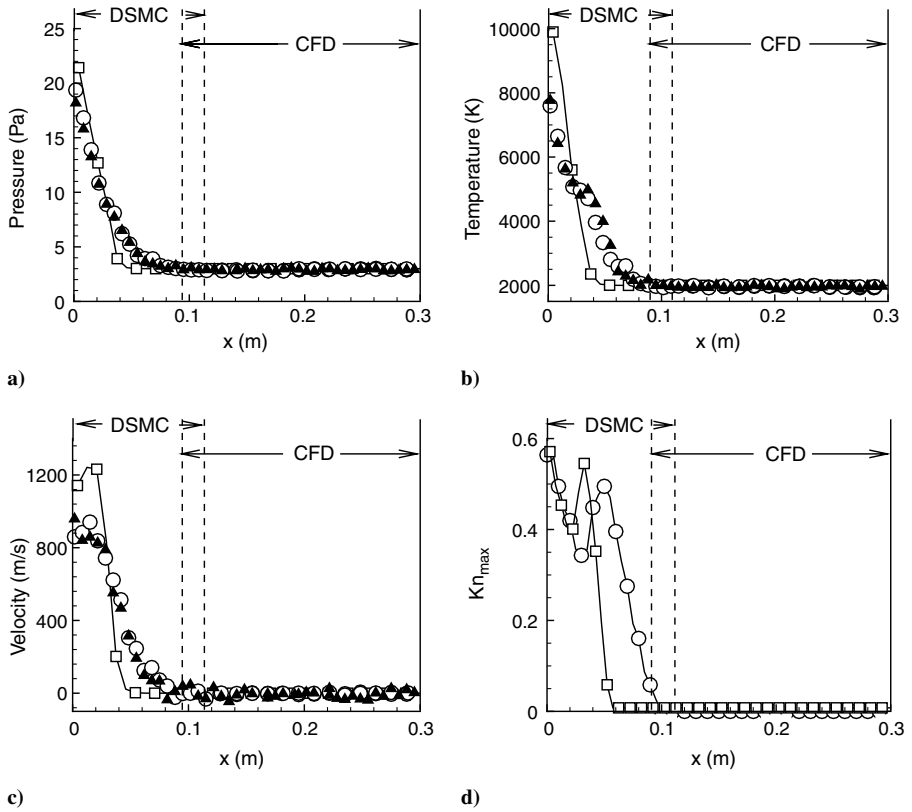

Fig. 4 Plots of a) pressure, b) temperature, c) velocity, and d) continuum breakdown parameter $Kn_{\max}$ in the tube after 1.5×10^{-5} s; CFD (□), DSMC (▲), and hybrid (○).

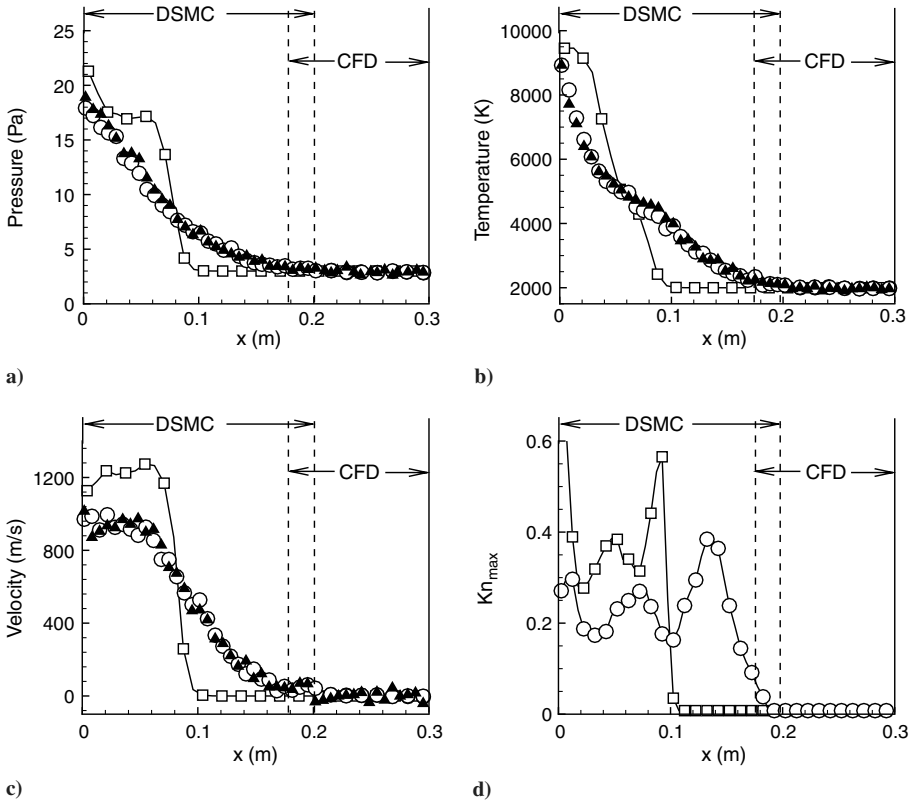

Fig. 5 Plots of a) pressure, b) temperature, c) velocity, and d) continuum breakdown parameter Kn_{max} in the tube after 3.0×10^{-5} s; CFD (□), DSMC (▲), and hybrid (○).

1. Sensitivity to Numerical Parameters

In this section, the sensitivity of the coupled approach to various numerical parameters is addressed for the 1-D shock-tube problem described in Sec. IV.A. In particular, the influence of the size of the overlap region, the DSMC noise, and the Courant number based on the time interval at which DSMC and CFD are coupled are analyzed.

a. Overlap Region. The sensitivity of our method to the size and position of the overlap region is investigated.

Both DSMC and N–S equations are solved in the overlap region (Fig. 2). The dependence of the results on the size of the overlap region is investigated by considering various overlap sizes: $\lambda/3$, 2λ, 6λ, and 12λ. In Sec. IV.A, an overlap size of 2λ is used.

Figure 6 shows the evolution in time of the shock velocity (Fig. 6a) and the shock thickness (Fig. 6b) evaluated using the different overlap sizes. From this figure, it is clear that the overlap size does not strongly influence the results of the simulation.

During this analysis, for all the considered sizes of the overlap region, two cases are tested: in the first, because the overlap is centered around the position at which $Kn = 0.05$, it could extend also into the $Kn > 0.05$ region, whereas in the second, the overlap is positioned such that it extended entirely in the $Kn < 0.05$ region. It is noted in the first case that if the overlap region is large, it is important to use an asymmetric overlap that is bounded on one side by the location at which $Kn = 0.1$. Otherwise, if the overlap region would extend into regions in which $Kn > 0.1$, the program would solve the N–S equations in a region in which the continuum hypotheses are no longer valid. As a result, instability problems appear (Fig. 7). The appearance of strong fluctuations due to instability produces two effects: the establishment of incorrect boundary conditions to both the CFD and DSMC solvers and an increase of the local gradients. The increase of the local gradients and the resulting reduction of the gradient length scales implies an incorrect determination of the CFD/DSMC interface. As a consequence, the CFD/DSMC interface rapidly moves into the low-Knudsen-number region and, together with the wrong boundary conditions, produces rapid propagation of the instability.

This section demonstrates an important advantage of the Schwarz coupling with Dirichlet–Dirichlet boundary conditions. Because of

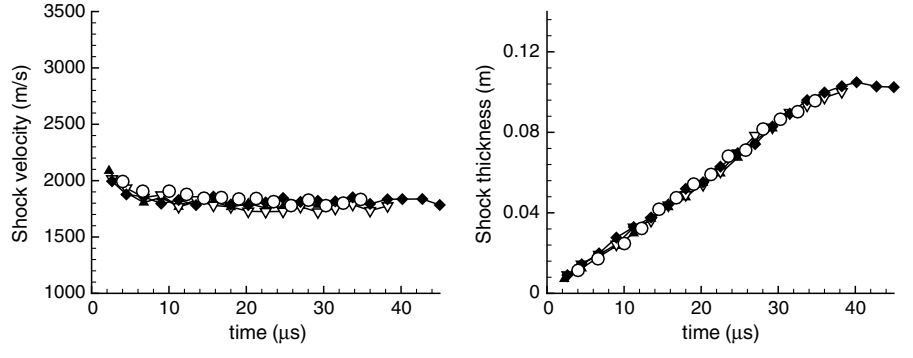

Fig. 6 Plots of a) computed shock velocity and b) shock thickness as a function of time for different sizes of the overlap region; $\lambda/3$ (▲), 2λ (▽), 6λ (◆), and 12λ (○).

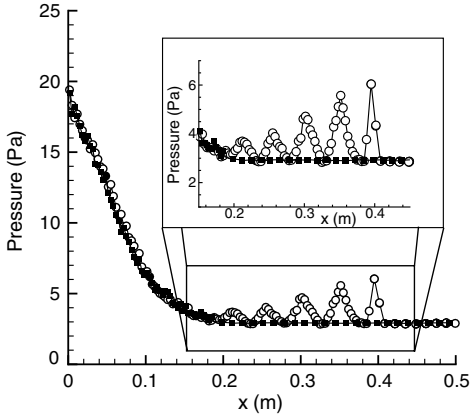

Fig. 7 Instability problems for an overlap region extending in the $Kn > 0.1$ region, overlap entirely in the $Kn < 0.1$ region (■), and overlap partially in the $Kn > 0.1$ region (○).

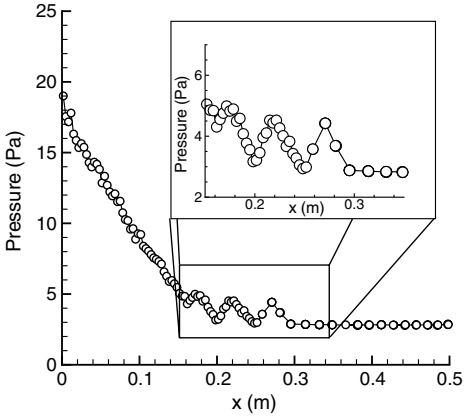

Fig. 9 Instability problems for Courant number $C = 1.46$.

the presence of an overlap region, the information exchange between CFD and DSMC does not take place at just one precise location, as in the flux-based coupling approaches [9–13]. For this reason, as long as we ensure that we run the CFD within its region of applicability ($Kn < 0.1$), the exact position and size of the overlap region are not crucial.

b. Number of Repeated Runs for the Ensemble Average. To analyze the effect of the noise in the DSMC solution on the coupling method, we considered different number of repeated runs for the ensemble average: 5, 30, and 50 runs.

From a comparison (not shown) of the evolution of the shock velocity and thickness, similar to that in Figure 6, it also became clear that the number of repeated runs over which we average does not strongly influence the results of the method.

The limited sensitivity of our method to the noise demonstrates a clear advantage of our Dirichlet–Dirichlet coupling method, as compared with flux-based coupling schemes [9–13], which show a strong sensitivity to noise.

c. Courant Number Based on the Coupling Time Step. In this section, we study the effect of varying the coupling Courant number defined as

$$C = C_r \frac{\Delta t_{\text{coupling}}}{\Delta x_{\text{CFD}}} \tag{5}$$

In Fig. 8, we present the evolution in time of both the shock velocity (Fig. 8a) and its thickness (Fig. 8b) for different coupling Courant numbers: 0.15, 0.24, 0.36, 0.73, and 1.46. To vary the Courant number with $C_r = 912$ m/s, we fixed $\Delta x_{\text{CFD}} = 0.005$ m and we considered different values of the coupling time step between 8.0×10^{-7} s and 8.0×10^{-6} s. In terms of multiples of the mean collision time, which is approximately $\Delta t_c = 6.0 \times 10^{-6}$ s, this corresponds to $0.13\Delta t_c$–$1.3\Delta t_c$. Only in the case in which the Courant number $C = 1.46 > 1$ is the solution found to deviate from the other solutions. In this case, in fact, the shock thickness is higher than for the other cases and the error is due to the appearance of instability effects (Fig. 9).

To be sure about the Courant number effect, we also varied the Courant number by varying Δx_{CFD} at fixed $\Delta t_{\text{coupling}}$ and fixed C_r and by varying C_r (through the temperature) at fixed Δx_{CFD} and $\Delta t_{\text{coupling}}$. In all cases, instabilities were found to arise when $C > 1$, as expected. It was therefore necessary to keep the Courant number smaller than 1.

This section demonstrates a further advantage of our overlapped Dirichlet–Dirichlet coupling method, as compared with flux-based coupling schemes [9–13]. In the flux-based coupling techniques, the impossibility of decoupling the continuum and molecular time scales imposes the necessity to run both the CFD and the DSMC with the molecular time step Δt_{DSMC}, which should be less than $0.1\Delta t_c$, and to couple them with that same time step. The Schwarz coupling, on the other hand, allows us to run the CFD and DSMC with their own time steps and to couple them every coupling time step $\Delta t_{\text{coupling}}$ as long as we respect the condition $C < 1$. In the present example, this led to $\Delta t_{\text{coupling}}$ up to $0.7\Delta t_c$, a gain of a factor ≈ 7, compared with $\Delta t_{\text{DSMC}} = 0.1\Delta t_c$.

B. Unsteady Pressure-Driven Slit Flow

To test our unsteady hybrid method in a multidimensional problem, it was applied to an unsteady pressure-driven slit flow test case (Fig. 10). The present test case is very similar to the test case used by Roveda et al. [11] to present their flux-based hybrid Euler/DSMC method without overlap.

We consider a jet of argon as it evolves following its initial burst from a slit of height $h = 0.05$ m in a wall at temperature $T_w = 500$ K. Before breaking, a membrane closes the slit, dividing two regions in which the fluid is in different conditions. In the left tank, it is at a pressure $P_1 = 16$ Pa and a temperature $T_1 = 500$ K, and the mean-free-path length is $\lambda_1 \approx 3.0 \times 10^{-4}$ m. In the

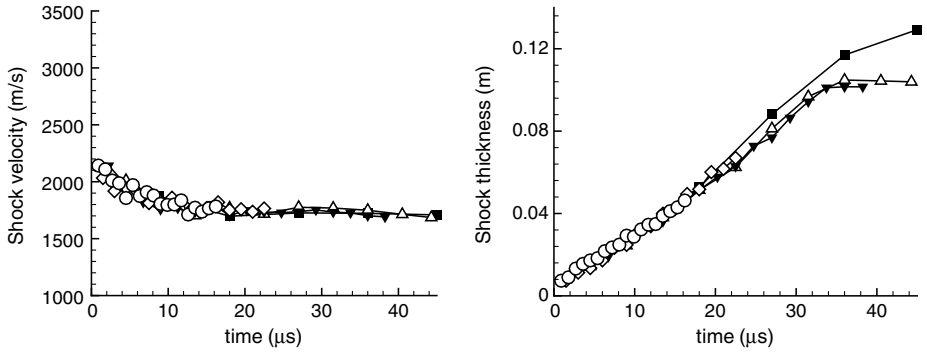

a) b)

Fig. 8 Plots of a) computed shock velocity and b) shock thickness for different coupling Courant numbers; $C = 1.46$ (■), $C = 0.73$ (△), $C = 0.36$ (▼), $C = 0.24$ (◇), and $C = 0.15$ (○).

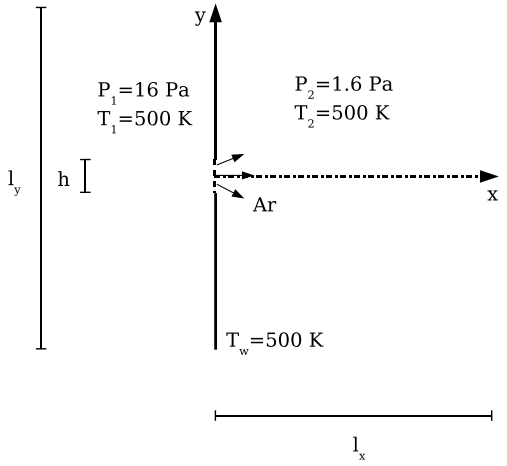

Fig. 10 Pressure-driven slit flow. The dashed line on the left indicates the membrane that is broken at the instant $t = 0$.

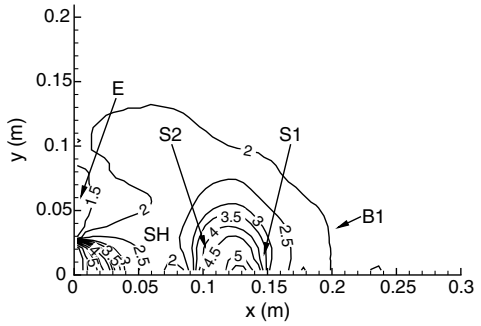

Fig. 11 Structure of the jet: density field (10^{-5} kg/m^3) in the jet after 5.25×10^{-4} s. Initial weak shock wave (B1), jet front (S1), normal shock (S2), shear layer (SH), and expansion region (E).

environment (right), it is at a pressure $P_2 = 1.6$ Pa and a temperature $T_2 = 500$ K, and the mean free path is $\lambda_2 \approx 0.003$ m.

At the instant $t = 0$, the membrane breaks, the gas can flow from left to right, and a complex jet structure begins to develop. Note that for the chosen pressure ratio $P_{1-2} = P_1/P_2 = 10$, a supersonic jet develops downstream the slit [11].

Figure 11 shows the density field after 5.25×10^{-4} s, as evaluated by a full DSMC simulation, illustrating the structure of the jet. In particular, note the initial weak shock wave (B1), the jet front (S1), a normal shock (S2), a shear layer (SH), and the starting evolution of an expansion region near the lips of the slit (E) according to the description in [11]. From symmetry considerations, we limit the simulation domain to the upper half of the flow domain, which extends for a length $l_x = 0.4$ m in the x direction and $l_y = 0.5$ m in the y direction.

The thermodynamic conditions inside the infinitely large left tank remain constant, and thus it can be modeled with an inlet boundary condition.

The initial grid is composed of 120 cells in the x direction and 60 cells in the y direction. The code automatically refines the mesh in the DSMC region to fulfill its requirements. The coupling time step is $\Delta t_{\text{coupling}} = 2.0 \times 10^{-6}$ s, which corresponds to a coupling Courant number $C \approx 0.75$. The ensemble averages of the DSMC solution were made on 50 repeated runs. In Fig. 12, the continuum breakdown parameter $Kn_{\max}$ in the jet is shown after 2.10×10^{-4} s (Fig. 12a) and 5.25×10^{-4} s (Fig. 12a), together with the division between the DSMC, CFD, and overlap regions in the hybrid CFD/DSMC approach. Outside the jet, because of the absence of gradients, gradient length scales are large and $Kn_{\max}$ (using local values of Q_{ref}) is low. In the complex structure of the jet, $Kn_{\max}$ is particularly high in the expansion region E (where the mean free path is higher), in the shocks (B1 and S2), and in the jet front (S1) because of the small gradient length scales due to the high gradients. In the hybrid CFD/DSMC approach, CFD is therefore particularly applied outside the jet, whereas the use of DSMC is especially required in the expansion E and in the region of the jet front S1 and the shock S2. Comparing Figs. 12c and 12d, it is possible to see the adaptation of the DSMC and CFD regions to the evolution of the flowfield.

In Fig. 13 the density fields evaluated by the hybrid CFD/DSMC approach after 2.10×10^{-4} s and 5.25×10^{-4} s are compared with the results of full DSMC and CFD simulations. The full DSMC solution is considered to be the most accurate of the three.

Comparing Figs. 13a–13f, respectively, one can see the evolution of the jet in time, predicted by the three methods. Note that the elements of the jet that are not clearly distinguishable after 2.10×10^{-4} s begin to have a clear shape and identity after 5.25×10^{-4} s.

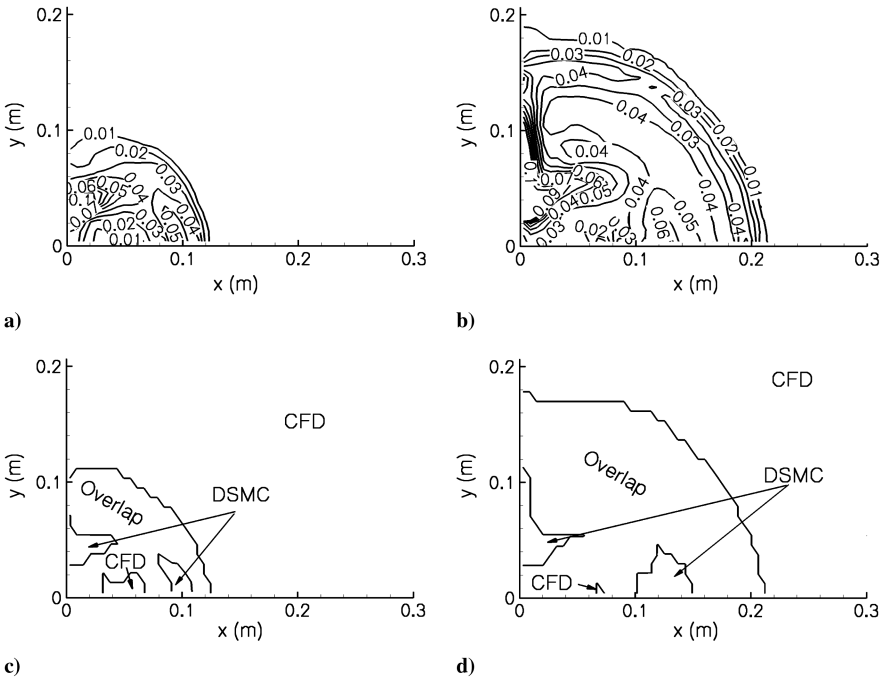

Fig. 12 Contours of the continuum breakdown parameter $Kn_{\max}$: a) after 2.10×10^{-4} s and b) after 5.25×10^{-4} s; CFD/DSMC domain splitting c) after 2.10×10^{-4} s and d) after 5.25×10^{-4} s.

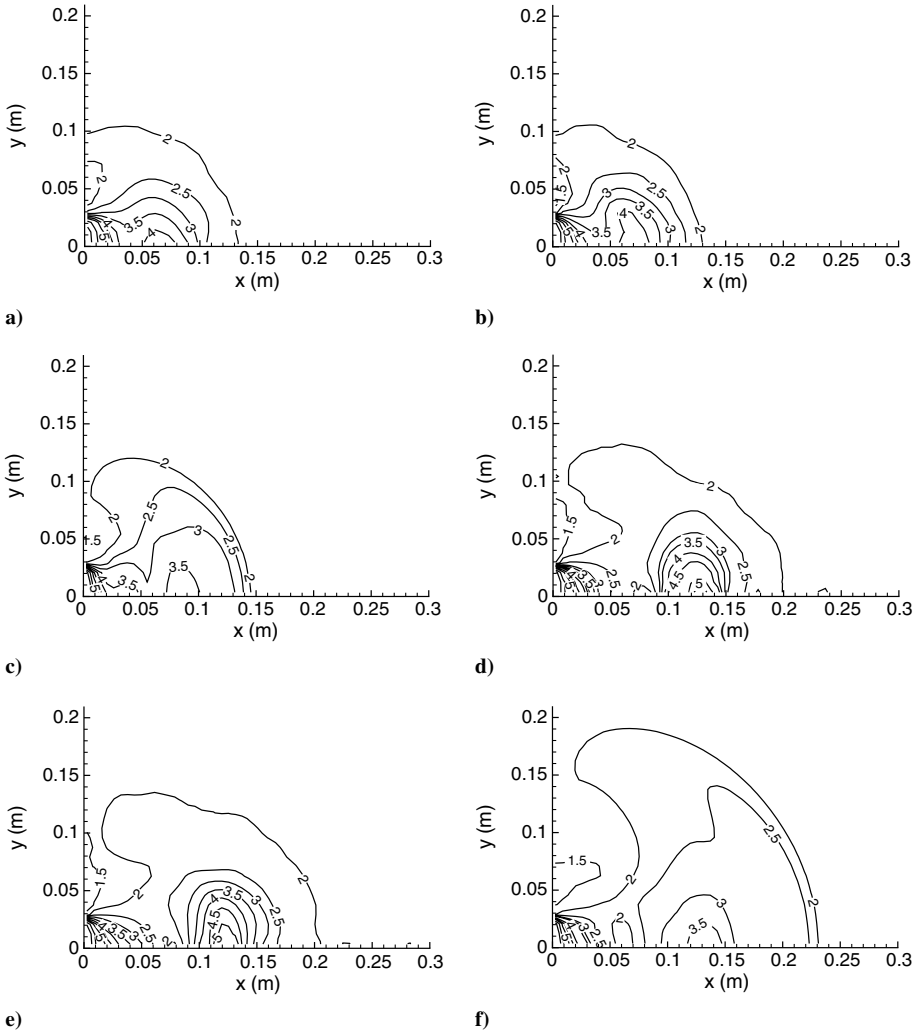

Fig. 13 Density field (10^{-5} kg/m^3) in the jet a) after 2.10×10^{-4} s evaluated by DSMC, b) hybrid simulations, and c) CFD; and d) after 5.25×10^{-4} s evaluated by DSMC, e) hybrid simulations, and f) CFD.

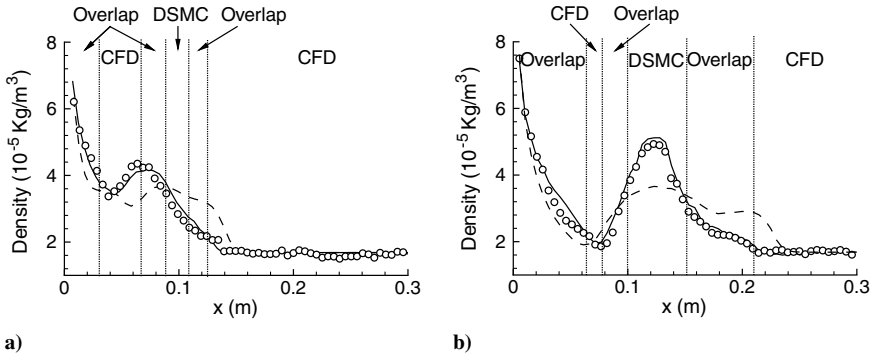

Fig. 14 Density profile along the x axis a) after 2.10×10^{-4} s and b) after 5.25×10^{-4} s; DSMC (○), hybrid simulations (solid line), and CFD (dashed line).

In Fig. 13, the hybrid method results in much better agreement with the DSMC than the full CFD simulations. The differences between the CFD and the other two methods increase in time, and after 5.25×10^{-4} s, the jet predicted by the CFD method covers a too-wide region and the density after the shock S2 is too low if compared with the DSMC results.

To have a more quantitative validation of the hybrid approach, Fig. 14 shows the density along the x axis for the hybrid method, the full CFD simulation, and the full DSMC simulation after 2.10×10^{-4} s (Fig. 14a) and 5.25×10^{-4} s (Fig. 14b). Although the results obtained with the hybrid approach are virtually identical to those obtained with the full DSMC solver, significant differences, which increase in time, can be observed between the full CFD and DSMC approaches. In particular, in the full CFD results, the jet travels slightly faster and the density after the shock S2 is lower.

Finally, the crucial fact to emphasize is that the hybrid results were obtained in ∼24 h on a single processor instead of the ∼250 h (∼1/10) of CPU time needed by the full DSMC method.

V. Conclusions

In this work, a hybrid continuum-rarefied method for multiscale flow simulation was presented. The method couples a compressible Navier–Stokes description of a macroscale continuum gas flow with

a molecular scale DSMC description of a rarefied gas flow in unsteady conditions. Transient simulations of a one-dimensional shock tube and a two-dimensional pressure-driven slit flow with the proposed method were successfully validated against full DSMC simulations. The results of the method were found to be independent of the size of the overlap region and the CFD/DSMC interface position as long as we ensure to run the CFD in the limits of its applicability ($Kn < 0.1$). The method also has limited sensitivity to noise, as demonstrated by its insensitivity to the number of DSMC runs for ensemble averaging to reduce scatter. However, to avoid instability effects, the coupling time step and the CFD cell size should be chosen such that the Courant number based on these quantities and on the molecular most-probable velocity is less than 1. These validation studies illustrate the potential of the method for transient, one-dimensional, and multidimensional flows.

References

[1] Sharipov, F., "Hypersonic Flow of Rarefied Gas Near the Brazilian Satellite During Its Re-Entry into Atmosphere," *Brazilian Journal of Physics*, Vol. 33, No. 2, 2003, pp. 398–405.

[2] Aktas, O., and Aluru, N. R., "A Combined Continuum/DSMC Technique for Multiscale Analysis of Microfluidic Filters," *Journal of Computational Physics*, Vol. 178, No. 2, 2002, pp. 342–372. doi:10.1006/jcph.2002.7030

[3] Cai, C., and Boyd, I. D., "3D Simulation of Plume Flows from a Cluster of Plasma Thrusters," 36th AIAA Plasmadynamics and Laser Conference, AIAA Paper 2005-4662, June 2005.

[4] Sanden, M. C. M. van de, Severens, R. J., Gielen, J. W. A. M., Paffen, R. M. J., and Schram, D. C., "Deposition of a-Si:H and a-C : H Using an Expanding Thermal Arc Plasma," *Plasma Sources Science and Technology* , Vol. 5, No. 2, 1996, pp. 268–274. doi:10.1088/0963-0252/5/2/022

[5] Hadjiconstantinou, N. G., "Hybrid Atomistic-Continuum Formulations and the Moving Contact-Line Problem," *Journal of Computational Physics*, Vol. 154, No. 2, 1999, pp. 245–265. doi:10.1006/jcph.1999.6302

[6] Kolobov, V. I., Arslanbekov, R. R., Aristov, V. V., Frolova, A. A., and Zabelok, S. A., "Unified Kinetic Approach for Simulation of Gas Flows in Rarefied and Continuum Regime," *Journal of Computational Physics*, Vol. 223, No. 2, 2007, pp. 589–608. doi:10.1016/j.jcp.2006.09.021

[7] Le Tallec, P., and Mallinger, F., "Coupling Boltzmann and Navier–Stokes Equations by Half Fluxes," *Journal of Computational Physics*, Vol. 136, No. 1, 1997, pp. 51–67. doi:10.1006/jcph.1997.5729

[8] Bourgat, J. F., Le Tallec, P., and Tidriri, M. D., "Coupling Boltzmann and Navier–Stokes Equations by Friction," *Journal of Computational Physics*, Vol. 127, No. 2, 1996, pp. 227–245. doi:10.1006/jcph.1996.0172

[9] Wijesinghe, H. S., and Hadjiconstantinou, N. G., "Discussion of Hybrid Atomistic-Continuum Methods for Multiscale Hydrodynamics," *International Journal of Multiscale Computational Engineering*, Vol. 2, No. 2, 2004, pp. 189–202. doi:10.1615/IntJMultCompEng.v2.i2.20

[10] Roveda, R., Goldstein, D. B., and Varghese, P. L., "Hybrid Euler/Particle Approach for Continuum/Rarefied Flows," *Journal of Spacecraft and Rockets*, Vol. 35, No. 3, 1998, pp. 258–265. doi:10.2514/2.3349

[11] Roveda, R., Goldstein, D. B., and Varghese, P. L., "Hybrid Euler/Direct Simulation Monte Carlo Calculation of Unsteady Slit Flow," *Journal of Spacecraft and Rockets*, Vol. 37, No. 6, 2000, pp. 753–760. doi:10.2514/2.3647

[12] Wijesinghe, H. S., Hornung, R. D., Garcia, A. L., and Hadjiconstantinou, N. G., "Three-Dimensional Continuum-Atomistic Simulations for Multiscale Hydrodynamics," *Journal of Fluids Engineering*, Vol. 126, No. 5, 2004, pp. 768–776. doi:10.1115/1.1792275

[13] Garcia, A. L., Bell, J. B., Crutchfield, W. Y., and Alder, B. J., "Adaptive Mesh and Algorithm Refinement Using Direct Simulation Monte Carlo," *Journal of Computational Physics*, Vol. 154, No. 1, 1999, pp. 134–155. doi:10.1006/jcph.1999.6305

[14] Glass, C. E., and Gnoffo, P. A., "A 3D Coupled CFD-DSMC Solution Method with Application to the Mars Sample Return Orbiter," NASA Langley Research Center TR NASA-2000-22isrgd-ceg, Hampton, VA, 2000.

[15] Wu, J. S., Lian, Y. Y., Cheng, G., Koomullil, R. P., and Tseng, K. C., "Development and Verification of a Coupled DSMC-NS Scheme Using Unstructured Mesh," *Journal of Computational Physics*, Vol. 219, No. 2, 2006, pp. 579–607. doi:10.1016/j.jcp.2006.04.013

[16] Schwartzentruber, T. E., Scalabrin, L. C., and Boyd, I. D., "Hybrid Particle-Continuum Simulation of Non-Equilibrium Hypersonic Blunt Body Flow Fields," *9th AIAA/ASME Joint Thermophisics and Heat Transfer Conference*, AIAA Paper 2006-3602, June 2006. doi:10.1016/j.jcp.2007.01.022

[17] Schwartzentruber, T. E., and Boyd, I. D., "A Hybrid Particle-Continuum Method Applied to Shock Waves," *Journal of Computational Physics*, Vol. 215, No. 2, 2006, pp. 402–416. doi:10.1016/j.jcp.2005.10.023

[18] Hash, D. B., and Hassan, H. A., "Two-Dimensional Coupling Issues of Hybrid DSMC/Navier–Stokes Solvers," AIAA Paper 97-2507, June 1997.

[19] Cheng, G. C., Koomullil, R. P., and Soni, B. K., "Multidisciplinary and Multi-Scale Computational Field Simulations Algorithms and Applications," *Mathematics and Computers in Simulation*, Vol. 75, No. 5, 2007, pp. 161–170. doi:10.1016/j.matcom.2006.12.007

[20] Wang, W. L., and Boyd, I. D., "Hybrid DSMC-CFD Simulations of Hypersonic Flow Over Sharp and Blunted Bodies," 36th AIAA Thermophysics Conference, AIAA Paper 2003-3644, June 2003.

[21] Carlson, A., Roveda, R., Boyd, I. D., and Candler, G. V., "A Hybrid CFD-DSMC Method of Modeling Continuum-Rarefied Flows," 42nd AIAA Aerospace Sciences Meeting and Exhibit, AIAA Paper 2004-1180, Jan. 2004.

[22] Schwartzentruber, T. E., Scalabrin, L. C., and Boyd, I. D., "A Modular Particle-Continuum Method for Hypersonic Non-Equilibrium Gas Flows," *Journal of Computational Physics*, Vol. 225, No. 1, 2007, pp. 1159–1171. doi:10.1016/j.jcp.2007.01.022

[23] Wang, W. L., and Boyd, I. D., "Continuum Breakdown in Hypersonic Viscous Flows," 40th AIAA Aerospace Sciences Meeting and Exhibit, AIAA Paper 2002-0651, Jan. 2002.

[24] Abbate, G., Thijsse, B. J., and Kleijn, C. R., "Validation of a Hybrid Navier–Stokes/DSMC Method for Multiscale Transient and Steady-State Gas Flows," *International Journal of Multiscale Computational Engineering*, Vol. 6, No. 1, 2008, pp. 1–12. doi:10.1615/IntJMultCompEng.v6.i1.10

[25] Abbate, G., Thijsse, B. J., Engeln, R., van de Sanden, M. C. M., Schram, D. C., and Kleijn, C. R., "Influence of Rarefaction on the Flow Dynamics of a Stationary Supersonic Hot-Gas Expansion," *Physical Review E (Statistical Physics, Plasmas, Fluids, and Related Interdisciplinary Topics)*, Vol. 77, No. 3, Pt. 2, 2008, Paper 036703. doi:10.1103/PhysRevE.77.036703

[26] Chou, S. Y., and Baganoff, D., "Kinetic Flux-Vector Splitting for the Navier–Stokes Equations," *Journal of Computational Physics*, Vol. 130, No. 2, 1997, pp. 217–230. doi:10.1006/jcph.1996.5579

[27] Lou, T., Dahlby, D. C., and Baganoff, D., "A Numerical Study Comparing Kinetic Flux-Vector Splitting for the Navier–Stokes Equations with a Particle Method," *Journal of Computational Physics*, Vol. 145, No. 2, 1998, pp. 489–510. doi:10.1006/jcph.1998.6040

[28] Hirschfelder, J. O., Curtis, C. F., and Bird, R. B., *Molecular Theory of Gasses and Liquids*, Wiley, New York, 1954.

[29] Bird, G. A., *Molecular Gas Dynamics and Direct Simulation Monte Carlo*, Clarendon, Oxford, 1998.

[30] Leer, B. van, "Towards the Ultimate Conservation Difference Scheme V, a Second Order Sequel to Gudunov's Method," *Journal of Computational Physics*, Vol. 32, No. 1, 1979, pp. 101–136. doi:10.1016/0021-9991(79)90145-1

[31] Sod, G. A., "A Survey of Several Finite Difference Methods for Systems of Nonlinear Hyperbolic Conservation Laws," *Journal of Computational Physics*, Vol. 27, No. 1, 1978, pp. 1–31. doi:10.1016/0021-9991(78)90023-2

[32] Harten, A., "High Resolution Schemes for Hyperbolic Conservation Laws," *Journal of Computational Physics*, Vol. 49, No. 3, 1983, pp. 357–393. doi:10.1016/0021-9991(83)90136-5

[33] Mott-Smith, H. M., "The Solution of the Boltzmann Equation for a Shock Wave," *Physical Review*, Vol. 82, No. 6, 1951, pp. 885–892. doi:10.1103/PhysRev.82.885

C. Kaplan
Associate Editor